Theoretical & Applied Mechanics Letters 8 (2018) 184-192

Contents lists available at ScienceDirect

Theoretical & Applied Mechanics Letters

journal homepage: www.elsevier.com/locate/taml

Letter

Nonlinear thermo-structural behavior of sandwich panels with truss cores under through-thickness gradient temperature field

Wu Yuan[a,b], Hongwei Song[a,b,*], Chenguang Huang[a,b]

[a] *Key Laboratory for Mechanics in Fluid Solid Coupling Systems, Institute of Mechanics, Chinese Academy of Sciences, Beijing 100190, China*
[b] *School of Engineering Science, University of Chinese Academy of Sciences, Beijing, 100049, China*

HIGHLIGHTS

- A theoretical model for sandwich panels with truss core under through-thickness gradient heating is proposed.
- Gradient shear and bending stiffness due to non-uniform temperature is considered.
- Nonlinear thermal bending in fixed inside surface temperature and thermal post-buckling in fixed temperature difference are analyzed.

ARTICLE INFO

Article history:
Received 18 October 2017
Received in revised form 18 January 2018
Accepted 5 February 2018
Available online 6 February 2018
*This article belongs to the Solid Mechanics.

Keywords:
Sandwich panel with truss core
Thermal protection system
Thermo-structural response
Nonlinear bending
Post-buckling

ABSTRACT

A theoretical analysis is presented to predict the nonlinear thermo-structural response of metallic sandwich panels with truss cores under through-thickness gradient temperature field, which is a common service condition for metallic thermal protection system (TPS). The in-plane temperature distribution is assumed to be uniform, and through-thickness temperature field is determined by heat conduction. Two typical conditions are analyzed: nonlinear thermal bending in fixed inside surface temperature, and thermal post-buckling in fixed temperature difference between two surfaces. Temperature-dependent mechanical properties are considered, and gradient shear stiffness and bending stiffness due to non-uniform temperature is included. Results indicate that the temperature-dependent material properties obviously affect bending resistance; however, the effect is negligible on post-buckling behavior. Influences of geometric parameters on the thermo-structural behavior of the sandwich panel according to the present theoretical model are discussed.

Sandwich panels are mechanically efficient lightweight structures that are composed of two thin and stiff face sheets and a relatively thick and lightweight porous core. Recently sandwich panels with truss cores (SPTCs) have been received considerable attention [1-12]. This type of structure has achieved significant success in various practical fields, such as heat insulation, energy absorption, noise reduction, and electromagnetic wave shield [2, 5, 13-15]. When being used in a thermal protection systems (TPS) of high-speed flight, the outside surface is typically subjected to intense aerodynamic heating, whereas the inside surface is approximated to an adiabatic boundary condition. Therefore, SPTCs constantly experience a through-thickness gradient temperature field due to heat conduction. One of the undesirable effects of SPTCs under such loadings is thermal stress, which may lead to premature failure at temperatures below those that substantially impair material properties [16]. Nonlinear thermal bending and thermal post-buckling are two main failure mechanisms in these conditions.

Ansari et al. [17] analyzed the nonlinear bending of a microplate based on Mindlin's strain gradient elasticity and first-order shear deformation plate theory. Le-Manh et al. [18] presented an analytical solution for the nonlinear bending behavior of a composite plate with variable thickness. For sandwich panels,

* Corresponding author.
E-mail address: songhw@imech.ac.cn (H.W. Song).

http://dx.doi.org/10.1016/j.taml.2018.03.007

Rezaeifard et al. [19] investigated the bending behavior of sandwich beams with elastic-plastic cores. Several studies have focused on the bending of plate structures subjected to thermal loadings. Suresh and Mortensen [20] considered the large deformation analysis of graded multi-layered composites. They found that the nonlinear strain-displacement relation should be applied when thermal loading reaches a high level. Shen [21, 22] analyzed the nonlinear thermal bending response of functionally graded material plates by using a two-step perturbation method. Dong and Li [23] developed a unified model for bending, buckling, and vibration for temperature-dependent functionally graded rectangular plates subjected to thermal loadings. Aside from theoretical analysis, numerical studies, such as those that use the weak form quadrature element method [24], the meshless method [25], and the element free Galerkin method [26], have also been conducted to investigate the bending response of thin-walled structures.

Cetkovic [27] investigated the critical thermal buckling behavior of laminated plates by using the layerwise displacement model. Yuan et al. [12] obtained the critical buckling temperatures of SPTCs under fully clamped boundary conditions based on the Ressiner model, later on they built failure maps considering thermal buckling as one of the failure modes [9]. For thermal post-buckling response, Mossavarali and Eslami [28] studied the thermal post-buckling behavior of thin plates with initial flaws. Nikrad and Asadi [29] provided a theoretical solution for the thermal post-buckling behavior of delaminated composite plates based on the minimum potential energy principle. Shen [30] investigated the thermal post-buckling behavior of a functionally graded plate based on high-order shear deformation theory. Yuan et al. [10] studied the thermal post-buckling behavior of SPTCs under uniform thermal loadings.

Few studies have examined the thermo-structural response of SPTCs when experience through-thickness gradient temperature field, which is a typical thermal loading condition for TPS during service. In the present work, the nonlinear thermal bending and thermal post-buckling behavior of SPTCs under through-thickness gradient temperature field are investigated. Through-thickness heat conduction and temperature-dependent material properties are considered, and gradient shear stiffness and bending stiffness due to non-uniform temperature is incorporated in the theoretical model.

Theoretical model. As shown in Fig. 1(a), a rectangular simply supported metallic SPTC is considered. The length, width, and thickness of the SPTC are a, b, and h_p, respectively. The thickness of the truss core is h_c. The angle between the core member and the face sheet is ω. A uniform heat flux due to aerodynamic heating is loaded onto the outside surface, and the inside surface approximates to an adiabatic boundary condition, as shown in Fig. 1(b). The in-plane temperature distribution is assumed to be uniform, and through-thickness temperature field is determined by heat conduction. Two cases of thermal boundary conditions are considered.

Case 1. The temperature of the inside face sheet T_i is assumed to be constant. In this case, the temperature difference between the two face sheets increases when it heated. Therefore, thermal bending is observed as the main failure mode.

Case 2. The temperature difference between the outside and inside face sheets $T_o - T_i$ is assumed to be constant. The thermal bending moment remains unchanged when the temperature of the SPTC varies. Hence, thermal post-buckling is the main failure mode.

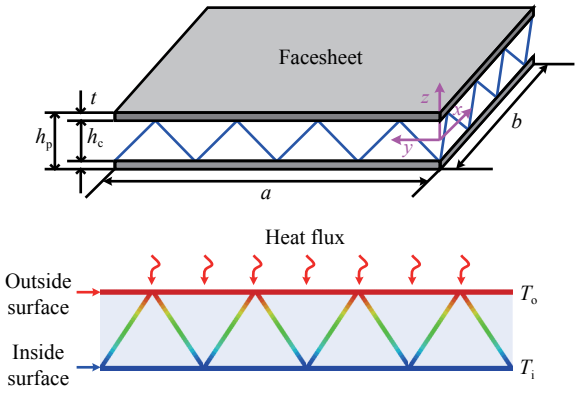

Fig. 1. Schematic of SPTCs under through-thickness gradient temperature field.

The through-thickness gradient temperature distribution can be obtained by solving a steady-state heat transfer equation as follows:

$$-\frac{\mathrm{d}}{\mathrm{d}Z}\left(k\frac{\mathrm{d}T}{\mathrm{d}Z}\right)=0. \tag{1}$$

The temperature distribution along the thickness of the face sheet is assumed to be uniform due to low thickness. Then, the temperature along the lengthwise direction of the truss member is solved by imposing the boundary conditions $T = T_i$ at $Z = -h_c/2$ and $T = T_o$ at $Z = h_c/2$ as follows:

$$T=\frac{T_i-T_o}{l_c}l+T_o. \tag{2}$$

The nonlinear equilibrium equations for SPTCs can be obtained by using the minimum potential principle, which can be expressed as

$$\frac{\partial N_X}{\partial X}+\frac{\partial N_{XY}}{\partial Y}=0, \tag{3}$$

$$\frac{\partial N_{XY}}{\partial X}+\frac{\partial N_Y}{\partial Y}=0, \tag{4}$$

$$\begin{aligned}&\frac{\partial Q_X}{\partial X}+\frac{\partial Q_Y}{\partial Y}+\frac{\partial}{\partial X}\left[N_X\frac{\partial(W+W_0)}{\partial X}+N_{XY}\frac{\partial(W+W_0)}{\partial Y}\right]\\&+\frac{\partial}{\partial Y}\left[N_{XY}\frac{\partial(W+W_0)}{\partial X}+N_Y\frac{\partial(W+W_0)}{\partial Y}\right]=0,\end{aligned} \tag{5}$$

$$\frac{\partial M_X}{\partial X}+\frac{\partial M_{XY}}{\partial Y}-Q_X=0, \tag{6}$$

$$\frac{\partial M_{XY}}{\partial X}+\frac{\partial M_Y}{\partial Y}-Q_Y=0. \tag{7}$$

The temperature-dependent material properties of the SPTC are considered, which can be written as

$$E=E(T), \tag{8}$$

where T is the temperature. The internal force is

$$N_X = \frac{[E(T_o)+E(T_i)](h_p-h_c)}{2(1-\mu^2)} \left\{\frac{\partial U}{\partial X}+\frac{1}{2}\left(\frac{\partial W}{\partial X}\right)^2+\frac{\partial W}{\partial X}\frac{\partial W_0}{\partial X} +\mu\left[\frac{\partial V}{\partial Y}+\frac{1}{2}\left(\frac{\partial W}{\partial Y}\right)^2+\frac{\partial W}{\partial Y}\frac{\partial W_0}{\partial Y}\right]\right\} - \frac{E(T_o)(1+\mu)\alpha(T_o-T_i)}{2}, \tag{9}$$

$$N_Y = \frac{[E(T_o)+E(T_i)](h_p-h_c)}{2(1-\mu^2)} \left\{\frac{\partial V}{\partial Y}+\frac{1}{2}\left(\frac{\partial W}{\partial Y}\right)^2+\frac{\partial W}{\partial Y}\frac{\partial W_0}{\partial Y} +\mu\left[\frac{\partial U}{\partial X}+\frac{1}{2}\left(\frac{\partial W}{\partial X}\right)^2+\frac{\partial W}{\partial X}\frac{\partial W_0}{\partial X}\right]\right\} - \frac{E(T_o)(1+\mu)\alpha(T_o-T_i)}{2}, \tag{10}$$

$$N_{XY} = \frac{[G(T_o)+G(T_i)](h_p-h_c)}{2} \left(\frac{\partial U}{\partial Y}+\frac{\partial V}{\partial X}+\frac{\partial W}{\partial X}\frac{\partial W}{\partial Y}+\frac{\partial W_0}{\partial X}\frac{\partial W}{\partial Y}+\frac{\partial W}{\partial X}\frac{\partial W_0}{\partial Y}\right), \tag{11}$$

$$M_X = D\left[\frac{\partial \psi_X}{\partial X}+\mu\left(\frac{\partial \psi_Y}{\partial Y}\right)\right]+M_T, \tag{12}$$

$$M_Y = D\left[\frac{\partial \psi_Y}{\partial Y}+\mu\left(\frac{\partial \psi_X}{\partial X}\right)\right]+M_T, \tag{13}$$

$$M_{XY} = \frac{(1-\mu)D}{2}\left(\frac{\partial \varphi_X}{\partial Y}+\frac{\partial \varphi_Y}{\partial X}\right), \tag{14}$$

$$M_T = \frac{E\alpha(h_p^2-h_c^2)(T_i-T_o)}{8(1-\mu)}, \tag{15}$$

$$Q_X = C\left(\psi_X+\frac{\partial W}{\partial X}\right), \tag{16}$$

$$Q_Y = C\left(\psi_Y+\frac{\partial W}{\partial Y}\right), \tag{17}$$

$$D = \frac{E(T_o)(h_p^3-h_c^3)}{24(1-\mu^2)}+\frac{E(T_i)(h_p^3-h_c^3)}{24(1-\mu^2)}, \tag{18}$$

$$C = G_c h_c, \tag{19}$$

where C and D are the shear stiffness and flexural rigidity of the sandwich panel, respectively.

The shear stiffness of the SPTC is derived by the equivalent shear deformation of a one-unit cell, as shown in Fig. 2. When the variation of the elastic modulus along the lengthwise direction of the truss member is considered, the truss core deformations of the pyramidal, tetrahedral, and Kagome configurations can be expressed as

$$\Delta_{\text{pyramid}} = \frac{E^* P}{2A\sin^2\omega}, \tag{20}$$

$$\Delta_{\text{tet}} = \frac{4E^* P}{3A\sin^2\omega}, \tag{21}$$

$$\Delta_{\text{Kagome}} = \frac{2E^* P}{3A\cos^2\omega}, \tag{22}$$

$$E^* = \int_0^{l_c}\frac{\mathrm{d}l}{E(l)}, \tag{23}$$

where A is the cross-sectional area of the truss member. The equivalent shear deformation of the truss cores subjected to a non-uniform thermal loading can be obtained as follows:

$$\gamma_{\text{pyramid}} = \frac{\Delta}{h_c} = \frac{E^* P}{2h_c A\sin^2\omega}, \tag{24}$$

$$\gamma_{\text{tet}} = \frac{\Delta}{h_c} = \frac{4E^* P}{3h_c A\sin^2\omega}, \tag{25}$$

$$\gamma_{\text{Kagome}} = \frac{\Delta}{h_c} = \frac{2E^* P}{3h_c A\cos^2\omega}. \tag{26}$$

Then, the equivalent shear modulus of the truss cores can be expressed as

$$G_{\text{pyramid}} = \frac{A\sin^2\omega}{E^* h_c}, \tag{27}$$

$$G_{\text{tet}} = \frac{A\sin^2\omega}{E^*\sqrt{3}h_c}, \tag{28}$$

$$G_{\text{Kagome}} = \frac{3h_c A\cos^2\omega}{2E^* h_d^2}. \tag{29}$$

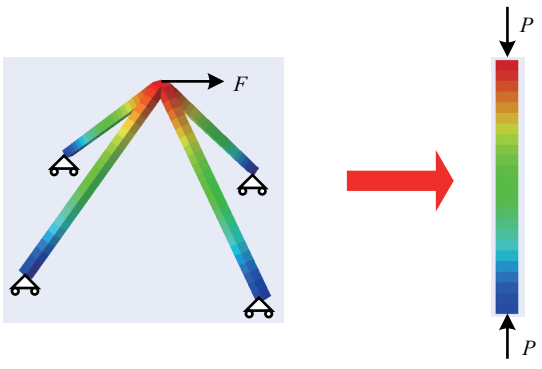

Fig. 2. Schematic of the thermal mechanical deformations of the pyramidal truss core member.

The relative density is

$$\overline{\rho}_{\text{tet}} = \frac{2\sqrt{3}A\sin\omega}{h_{\text{c}}^2}, \tag{30}$$

$$\overline{\rho}_{\text{pyramid}} = \frac{4A\sin\omega}{h_{\text{c}}^2}, \tag{31}$$

$$\overline{\rho}_{\text{Kagome}} = \frac{3A}{h_{\text{d}}^2\sin\omega}, \tag{32}$$

where h_{d} is the distance between the truss core elements of the Kagome configuration. The pyramidal, tetrahedral, and Kagome configurations are 45°, 55.7°, and 55.7°, respectively. Finally, the shear stiffness of the sandwich panel can be derived.

$$C_{\text{pyramid}}=G_{\text{pyramid}}h_{\text{c}} = \frac{h_{\text{c}}^2\bar{\rho}}{4E^*}\sin\omega = \frac{\sqrt{2}}{8E^*}\bar{\rho}h_{\text{c}}^2, \tag{33}$$

$$C_{\text{tet}}=G_{\text{tet}}h_{\text{c}} = \frac{1}{6E^*}\bar{\rho}h_{\text{c}}^2\sin\omega = \frac{\sqrt{2}}{6\sqrt{3}E^*}\bar{\rho}h_{\text{c}}^2, \tag{34}$$

$$C_{\text{Kagome}} = G_{\text{Kagome}}h_{\text{c}} = \frac{1}{2E^*}\bar{\rho}h_{\text{c}}^2\cos^2\omega\sin\omega = \frac{\sqrt{2}}{6\sqrt{3}E^*}\bar{\rho}h_{\text{c}}^2. \tag{35}$$

Analytical method. When stress functions and deformation compatibility are considered, the dimensionless differential governing equations for the SPTC subjected to non-uniform through-thickness loadings can be obtained by introducing the dimensionless quantities used in Ref. [10].

$$\bar{\nabla}^4F = \beta^2\gamma^2\left[\left(\frac{\partial^2w}{\partial x\partial y}\right)^2 - \frac{\partial^2w}{\partial x^2}\frac{\partial^2w}{\partial y^2} + 2\frac{\partial^2w_0}{\partial x\partial y}\frac{\partial^2w}{\partial x\partial y} - \frac{\partial^2w}{\partial x^2}\frac{\partial^2w_0}{\partial y^2} - \frac{\partial^2w}{\partial y^2}\frac{\partial^2w_0}{\partial x^2}\right], \tag{36}$$

$$\frac{\partial\varphi_x}{\partial x} + \beta\frac{\partial\varphi_y}{\partial y} + \bar{\nabla}^2w + \phi^2\frac{\partial}{\partial x}\left[\frac{\partial^2F}{\partial y^2}\frac{\partial(w+w_0)}{\partial x} - \frac{\partial^2F}{\partial x\partial y}\frac{\partial(w+w_0)}{\partial y}\right] + \phi^2\frac{\partial}{\partial y}\left[\frac{\partial^2F}{\partial x^2}\frac{\partial(w+w_0)}{\partial y} - \frac{\partial^2F}{\partial x\partial y}\frac{\partial(w+w_0)}{\partial x}\right] = 0, \tag{37}$$

$$\eta^2\left(\frac{\partial^2\varphi_x}{\partial x^2} + \mu\beta\frac{\partial^2\varphi_y}{\partial x\partial y}\right) + \frac{\partial m_T}{\partial x} + \frac{(1-\mu)\eta^2}{2}\left(\beta^2\frac{\partial^2\varphi_x}{\partial y^2} + \beta\frac{\partial^2\varphi_y}{\partial x\partial y}\right) - \varphi_x - \frac{\partial w}{\partial x} = 0, \tag{38}$$

$$\eta^2\left(\beta^2\frac{\partial^2\varphi_y}{\partial y^2} + \mu\beta\frac{\partial^2\varphi_x}{\partial x\partial y}\right) + \frac{\partial m_T}{\partial y} + \frac{(1-\mu)\eta^2}{2}\left(\frac{\partial^2\varphi_y}{\partial x^2} + \beta\frac{\partial^2\varphi_x}{\partial x\partial y}\right) - \varphi_y - \beta\frac{\partial w}{\partial y} = 0, \tag{39}$$

where

$$\bar{\nabla}^2 = \frac{\partial^2}{\partial x^2} + \beta^2\frac{\partial^2}{\partial y^2}, \tag{40}$$

$$\bar{\nabla}^4 = \frac{\partial^4}{\partial x^4} + 2\beta^2\frac{\partial^2}{\partial x^2\partial y^2} + \beta^4\frac{\partial^4}{\partial y^4}, \tag{41}$$

$$m_T = \frac{E\alpha\sqrt{12(1-\mu^2)}(h_{\text{p}}^2 - h_{\text{c}}^2)(T_{\text{d}} - T_{\text{u}})}{8Ch_{\text{p}}(1-\mu)}. \tag{42}$$

The thermal bending moment can be expanded in the double Fourier sine series as

$$m_T = -m_0\sum_{i=1,3,\ldots}\sum_{j=1,3,\ldots}\frac{1}{ij}\sin(ix)\sin(jy). \tag{43}$$

Equations. (36)–(39) can be solved by applying the two-step perturbation technique used in Ref. [30]. The solutions for the unknown functions are assumed to have the following forms:

$$w(x,y,\varepsilon) = \sum_{i=1}\varepsilon^iw_i(x,y), \quad F(x,y,\varepsilon) = \sum_{i=0}\varepsilon^iF_i(x,y), \tag{44}$$

$$\varphi_x(x,y,\varepsilon) = \sum_{i=1}\varepsilon^i\varphi_{xi}(x,y), \quad \varphi_y(x,y,\varepsilon) = \sum_{i=1}\varepsilon^i\varphi_{yi}(x,y), \tag{45}$$

where ε is the small perturbation parameter. The first term of the out-of-plane displacement is assumed to have the following form:

$$w_1(x,y) = A_{11}\sin(mx)\sin(ny). \tag{46}$$

The initial global geometric imperfection of the SPTC can be expressed in the following form:

$$w_0(x,y) = \varepsilon\lambda A_{11}\sin(mx)\sin(ny). \tag{47}$$

Equations. (44)–(45) can be solved by substituting Eqs. (43)–(47) into Eqs. (36)–(39) and collecting terms with the same order as ε.

$$w(x,y,\varepsilon) = \varepsilon[A_{11}\sin(mx)\sin(ny)] + \varepsilon^3[A_{13}\sin(mx)\sin(3ny) + A_{31}\sin(3mx)\sin(ny)] + O(\varepsilon^5), \tag{48}$$

$$\varphi_x(x,y,\varepsilon) = \varepsilon[C_{11}\cos(mx)\sin(ny)] + \varepsilon^3[C_{13}\cos(mx)\sin(3ny) + C_{31}\cos(3mx)\sin(ny)] + O(\varepsilon^5), \tag{49}$$

$$\varphi_y(x,y,\varepsilon) = \varepsilon[D_{11}\sin(mx)\cos(ny)] + \varepsilon^3[D_{13}\sin(mx)\cos(3ny) + D_{31}\sin(3mx)\cos(ny)] + O(\varepsilon^5), \tag{50}$$

$$\begin{aligned}F(x,y,\varepsilon) = {} & -B_{100}\frac{y^2}{2} - b_{100}\frac{x^2}{2} + \varepsilon^2\left[-B_{200}\frac{y^2}{2} - b_{200}\frac{x^2}{2} + B_{220}\cos(2mx) + B_{202}\cos(2ny)\right] \\ & + \varepsilon^4\left[-B_{400}\frac{y^2}{2} - b_{400}\frac{x^2}{2} + B_{420}\cos(2mx) + B_{402}\cos(2ny) + B_{422}\cos(2mx)\cos(2ny) + B_{440}\cos(4mx) + B_{404}\cos(4ny) + B_{424}\cos(2mx)\cos(4ny) + B_{442}\cos(4mx)\cos(2ny)\right] + O(\varepsilon^5).\end{aligned} \tag{51}$$

The symbols used in Eqs.(48)-(51) are described in Appendix A.

When Eqs. (48)–(51) is substituted into the simply supported boundary conditions, the equilibrium path of the SPTC subjected to non-uniform through-thickness heating can be obtained by

$$\Omega_T = \Omega_{10} + \Omega_{12} w_m^2 + \Omega_{14} w_m^4. \tag{52}$$

All the symbols used in Eq. (52) are described in Appendix B.

The theoretical results of the response of SPTCs subjected to non-uniform through-thickness heating are presented here. The mechanical properties of a metallic material are degraded with an increase in temperature. Therefore, temperature-dependent material properties are considered in the theoretical model. In the present study, stainless steel is selected for the SPTC. The elastic modulus of stainless steel can be expressed as a quadratic function of temperature as follows:

$$E(T) = P_0 + P_1 T + P_2 T^2, \tag{53}$$

where P_0, P_1, and P_2 are the coefficients of the quadratic function, as shown in Table 1. The thermal expansion coefficient of stainless steel α is 1.7×10^{-5}°C^{-1}. To obtain the response of SPTCs with temperature-dependent materials, Eq. (52) is solved using an iterative numerical procedure. Then, the effects of geometric and material properties on the nonlinear thermal bending and thermal post-buckling behavior of SPTCs are investigated.

Nonlinear thermal bending. Figure 3 shows the effect of geometric parameters on the nonlinear thermal bending behavior of SPTCs with different configurations. "TD" denotes SPTCs with temperature-dependent materials, whereas "T-ID" denotes temperature-independent materials. In Case 1, the temperature of the inside surface is assumed to be constant, which is 20°C, whereas the temperature of the outside surface increases with an increase in heat flux irradiation time. Under this condition, ΔT indicates the temperature increase of the outside face sheet. The in-plane force produced by thermal stresses in the outside face sheet will decrease when temperature-dependent material properties are considered, whereas the stiffness of the inside surface will remain in its initial state. Consequently, the bending deformation of the SPTC with TD materials is smaller than that of the SPTC with T-ID materials when they exhibit the same temperature increase, as shown in Fig. 3(a).

As indicated in Eq. (33)–(35), the shear stiffness of the SPTC is proportional to relative density. Therefore, increasing relative density will increase the stiffness of the SPTC under thermal bending. Among the three configurations, the shear modulus of the SPTC with a pyramidal truss cores is larger than those of the two other configurations. Consequently, bending resistance of the sandwich panel with pyramidal truss cores under nonlinear bending is the highest among the three configurations. However, the difference among the three configurations is not evident when relative density increases.

As shown in Fig. 3(b), aspect ratio β significantly affects the nonlinear thermal bending behavior of the SPTC. The slenderness ratio of the SPTC is increased with an increase in aspect ratio β. Therefore, the stiffness to thermal bending is decreased. The variation in thickness may significantly affect the flexural stiffness and in-plane load of the SPTC. Consequently, the effect of face sheet thickness on the bending behavior of the SPTC dif-

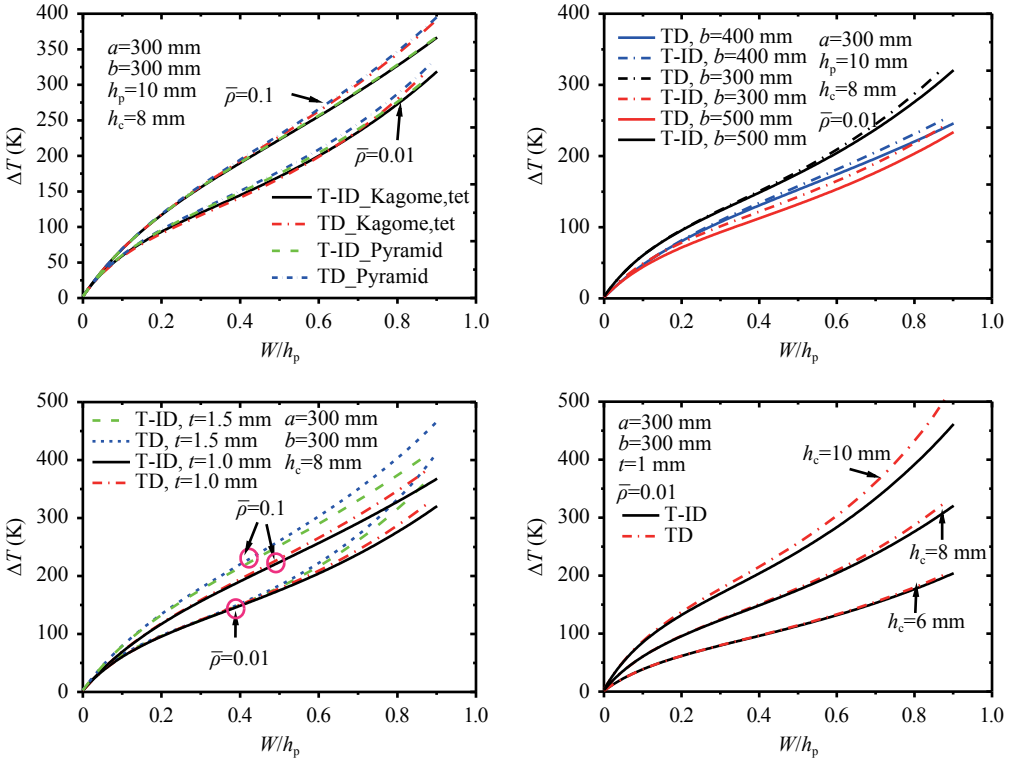

Fig. 3. Effect of geometric parameters on the nonlinear bending behavior of SPTCs under through-thickness gradient temperature field, $T_i = 20$°C.

fers when relative density varies. As shown in Fig. 3(c), the stiffness under thermal bending of the SPTC with a thicker face sheet is evidently higher even under a small thermal loading when relative density is 0.1. However, the shear stiffness of the SPTC is lower when relative density decreases to 0.01. In such case, increasing the thickness of the face sheet will simultaneously increase the in-plane compressive force. Therefore, the bending resistance of the SPTC is not increased significantly. Figure 3(d) shows the effect of sandwich panel thickness h_c on the nonlinear thermal bending behavior of the sandwich panel with pyramidal truss cores. The results indicate that the bending resistance of the SPTC is improved when the thickness of the sandwich panel is increased.

Thermal-post buckling. In Case 2, a fixed through-thickness temperature increase is observed and ΔT denotes the temperature increase of the sandwich panel. If temperature-dependent material properties are considered, then the thermal bending moment is decreased when the temperature rise of the SPTC increases. Therefore, thermal post-buckling will be the main failure mode under this type of thermal boundary condition.

Figure 4 shows the thermal post-buckling behaviour of the SPTC under different relative densities. Unlike in the nonlinear thermal bending behavior, the elastic modulus of the two face sheets decreases when temperature increases. The degradation of the in-plane force and stiffness of the SPTC can be canceled out. Therefore, the post-buckling deformation of the SPTC with TD materials is in accordance with that of the SPTC with T-ID materials, as shown in Fig. 4(a). In addition, the buckling deformation of sandwich panels with pyramidal truss cores is smaller than those of the other two configurations when they have the same relative density. Similarly, the thermal buckling deformation of the SPTC with a relative density of 0.1 is smaller than that of the SPTC with a relative density of 0.01. Figure 4(b) shows the effect of temperature gradient on the thermal post-buckling behavior of SPTCs. SPTCs will exhibit an initial bend-

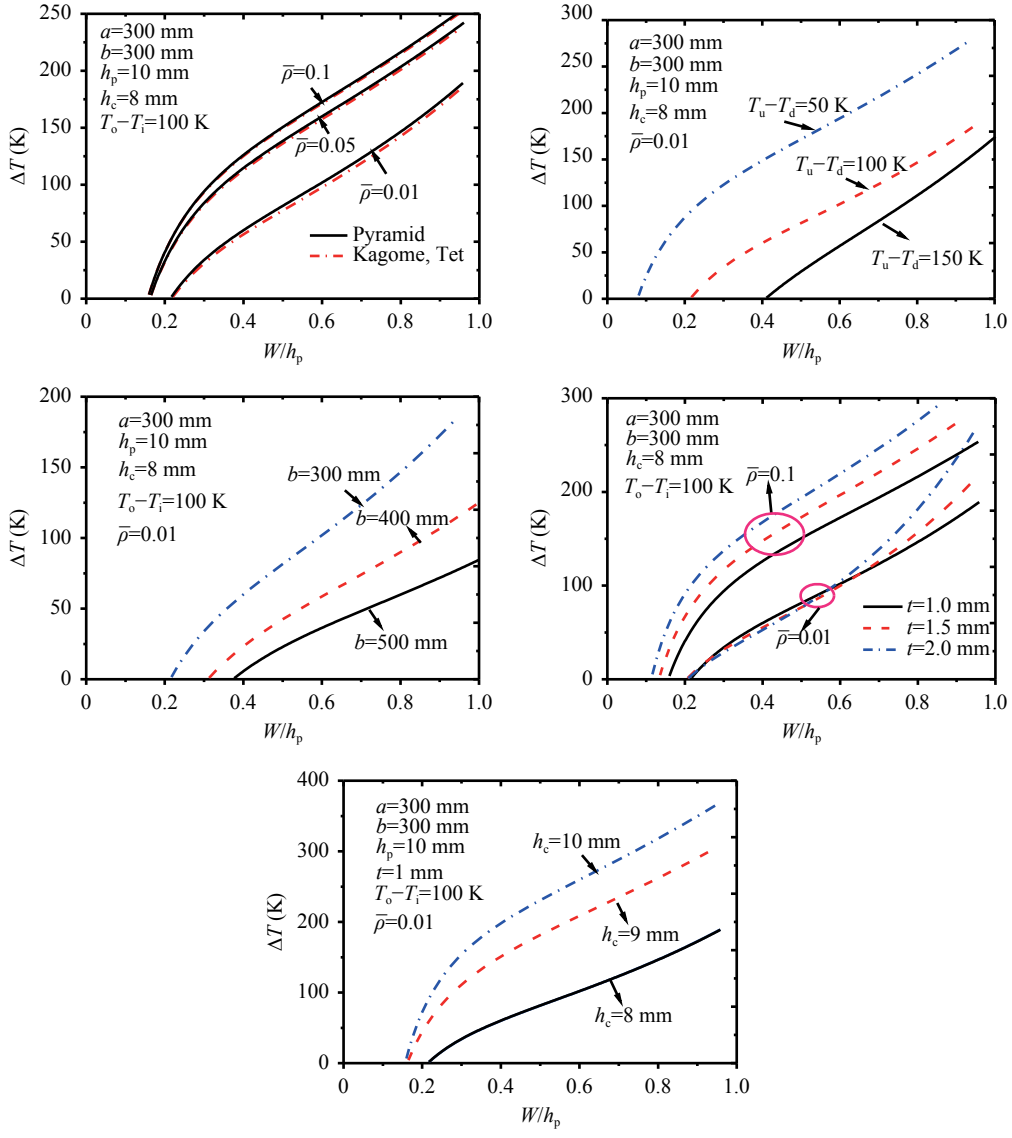

Fig. 4. Effect of geometric parameters on the thermal post-buckling behavior of SPTCs under through-thickness gradient temperature field.

ing deformation at the onset due to the thermal bending moment induced by the initial through-thickness temperature gradient. Therefore, the initial temperature gradient will considerably influence the buckling behaviour of SPTCs.

The bending resistance is decreased with an increase in the length of one side of the SPTC, as shown in Fig. 4(c). Similar to thermal bending response, the effect of face sheet thickness on the thermal post-buckling behavior of the SPTC subjected to non-uniform through-thickness heating differs when relative density varies. Figure 4(d) shows that the stiffness of the SPTC with a thicker face sheet is higher when relative density is 0.1. However, an increase in thickness may reduce bending resistance of the SPTC when relative density decreases to 0.01. Figure 4(e) shows the effect of sandwich panel thickness h_c on the thermal post-buckling behaviour of the SPTC. Equation (18) indicates that the flexural stiffness of the SPTC is significantly increased with an increase in thickness. Therefore, the the thermal post-buckling resistance can be improved by using a thick sandwich panel.

The response of simply supported SPTCs under through-thickness gradient temperature filed is investigated theoretically. The nonlinear equilibrium equations for SPTCs are developed by applying the minimum potential energy principle. The equilibrium path is obtained by using the perturbation approach. Nonlinear thermal bending and thermal post-buckling are evaluated. The effects of geometric and material properties on the response of the SPTC are investigated. The deformation of the SPTC is small for the thermal bending behavior when temperature-dependent properties are considered. Meanwhile, temperature-dependent properties have minimal effects on the thermal post-buckling behavior. The stiffness of the sandwich panel with pyramidal truss cores is higher than those of the Kagome and tetrahedral configurations. The SPTC under thermal bending and post-buckling resistance can be improved by applying a high relative density. The stiffness of the SPTC subjected to non-uniform through-thickness heating is increased with an increase in sandwich panel thickness. The effect of face sheet thickness differs when relative density varies.

Acknowledgments

The financial support from the National Natural Science Foundation of China (91016025, 11472276, 11602271, and 11332011) and the Defense Industrial Technology Development Program of China (JCKY2016130B009) is gratefully acknowledged.

Appendix A

$$C_{11}=\frac{(m+m_t)k_{22}-(\beta n+m_t)k_{12}}{k_{11}k_{22}-k_{12}k_{21}}A_{11},$$

$$D_{11}=\frac{(\beta n+m_t)k_{11}-(m+m_t)k_{21}}{k_{11}k_{22}-k_{12}k_{21}}A_{11},$$

$$A_{13}=f_2(\zeta_{33}\zeta_{55}-\zeta_{35}\zeta_{53})/\chi_1,$$

$$A_{31}=f_1(\zeta_{44}\zeta_{66}-\zeta_{46}\zeta_{64})/\chi_2,$$

$$C_{13}=-f_2(\zeta_{31}\zeta_{55}-\zeta_{35}\zeta_{51})/\chi_1,$$

$$C_{31}=-f_1(\zeta_{42}\zeta_{66}-\zeta_{46}\zeta_{62})/\chi_2,$$

$$D_{13}=f_2(\zeta_{31}\zeta_{53}-\zeta_{33}\zeta_{51})/\chi_1,$$

$$D_{31}=f_1(\zeta_{42}\zeta_{64}-\zeta_{44}\zeta_{62})/\chi_2,$$

$$B_{100}=\frac{1}{\phi^2(1+\lambda)(m^2+n^2\beta^2)}\left[m\,\frac{(m+m_t)k_{22}-(\beta n+m_t)k_{12}}{k_{11}k_{22}-k_{12}k_{21}}+\beta n\,\frac{(\beta n+m_t)k_{11}-(m+m_t)k_{21}}{k_{11}k_{22}-k_{12}k_{21}}+m^2+\beta^2n^2\right],$$

$$b_{100}=\beta^2B_{100},$$

$$B_{200}=\frac{1}{m^2+n^2}\left\{2m^2n^2\left[\frac{n^2(1+2\lambda)\beta^2\gamma^2}{32m^2}A_{11}^2+\frac{m^2(1+2\lambda)\gamma^2}{32n^2\beta^2}A_{11}^2\right]-\frac{(\gamma^2+2\lambda)(\beta^2n^2-m^2)}{8(1+\mu)}A_{11}^2\right\},$$

$$b_{200}=\beta^2B_{200}+\frac{(\gamma^2+2\lambda)(\beta^2n^2-m^2)}{8(1+\mu)}A_{11}^2,$$

$$B_{400}=\frac{2\phi^2m^2n^2(B_{202}A_{13}+B_{220}A_{31})}{A_{11}(1+\lambda)(m^2\phi^2+\beta^2n^2\phi^2)},$$

$$b_{400}=\beta^2B_{400},$$

$$B_{420}=-\frac{16n^2\beta^2\gamma^2(1+\lambda)A_{11}A_{31}}{m^2},$$

$$B_{422}=-\frac{4m^2n^2\beta^2\gamma^2(1+\lambda)A_{11}(A_{31}+A_{13})}{16m^4+32m^2n^2\beta^2+n^4\beta^4},$$

$$B_{440}=-\frac{n^2\beta^2\gamma^2(1+\lambda)A_{11}A_{31}}{64m^2},$$

$$B_{424}=-\frac{m^2n^2\beta^2\gamma^2(1+\lambda)A_{11}A_{13}}{16m^4+128m^2n^2\beta^2+256n^4\beta^4},$$

$$B_{442}=-\frac{m^2n^2\beta^2\gamma^2(1+\lambda)A_{11}A_{13}}{256m^4+128m^2n^2\beta^2+16n^4\beta^4},$$

$$B_{402}=-\frac{m^2n^2\gamma^2(1+\lambda)A_{11}A_{31}}{16n^2\beta^2},$$

$$B_{404}=\frac{m^2n^2\gamma^2(1+\lambda)A_{11}A_{31}}{64n^2\beta^2}.$$

Appendix B

$$\Omega_T=\xi\alpha\Delta T,$$

$$\Omega_{10}=\frac{(1-\mu)\beta^2}{\gamma^2\phi^2(1+\lambda)(m^2+n^2\beta^2)}\left[m\,\frac{(m+m_t)k_{22}-(\beta n+m_t)k_{12}}{k_{11}k_{22}-k_{12}k_{21}}\right.$$
$$\left.+\beta n\,\frac{(\beta n+m_t)k_{11}-(m+m_t)k_{21}}{k_{11}k_{22}-k_{12}k_{21}}+m^2+\beta^2n^2\right],$$

$$\Omega_{12}=\frac{1}{8}(1+2\lambda)\,m^2+\frac{1}{\gamma^2}\left\{\frac{\beta^2(1-\mu)}{m^2+n^2}\left\{2m^2n^2\left[\frac{n^2(1+2\lambda)\beta^2\gamma^2}{32m^2}\right.\right.\right.$$
$$\left.+\frac{m^2(1+2\lambda)\gamma^2}{32n^2\beta^2}\right]-\frac{(\gamma^2+2\lambda)(\beta^2n^2-m^2)}{8(1+\mu)}\Bigg\}$$
$$\left.+\frac{(\gamma^2+2\lambda)(\beta^2n^2-m^2)}{8(1+\mu)}\right\},$$

$$\Omega_{14}=\frac{\beta^2(1-\mu)}{\gamma^2}\,\frac{2\phi^2m^2n^2}{(1+\lambda)(m^2\phi^2+\beta^2n^2\phi^2)}$$
$$\left[\frac{n^2(1+2\lambda)\beta^2\gamma^2}{32m^2}\,\frac{(1+\lambda)(1+2\lambda)m^4\phi^2\gamma^2}{16\beta^2}\,\Lambda_{13}\right.$$
$$\left.+\frac{m^2(1+2\lambda)\gamma^2}{32n^2\beta^2}\,\frac{(1+2\lambda)(1+\lambda)\beta^2n^4\phi^2\gamma^2}{16}\,\Lambda_{31}\right]$$
$$+2\Omega_{12}\left[\frac{(1+\lambda)(1+2\lambda)m^4\phi^2\gamma^2}{16\beta^2}\,\Lambda_{13}\right.$$
$$\left.+\frac{(1+2\lambda)(1+\lambda)\beta^2n^4\phi^2\gamma^2}{16}\,\Lambda_{31}\right].$$

References

[1] V.S. Deshpande, N.A. Fleck, Collapse of truss core sandwich beams in 3-point bending, Int. J. Solids Struct. 38 (2001) 6275–6305.

[2] K.P. Dharmasena, H.N.G. Wadley, K. Williams, et al., Response of metallic pyramidal lattice core sandwich panels to high intensity impulsive loading in air, Int. J. Impact Eng. 38 (2011) 275–289.

[3] S. Hyun, A.M. Karlsson, S. Torquato, et al., Simulated properties of Kagome and tetragonal truss core panels, Int. J. Solids Struct. 40 (2003) 6989–6998.

[4] W.C. Jiang, H. Chen, J.M. Gong, et al., Numerical modelling and nanoindentation experiment to study the brazed residual stresses in an X-type lattice truss sandwich structure, Mat. Sci. Eng. A 528 (2011) 4715–4722.

[5] M. Li, L.Z. Wu, L. Ma, et al., Structural response of all-composite pyramidal truss core sandwich columns in end compression, Compos. Struct. 93 (2011) 1964–1972.

[6] J.S. Park, J.H. Joo, B.C. Lee, et al., Mechanical behaviour of tube-woven Kagome truss cores under compression, Int. J. Mech. Sci. 53 (2011) 65–73.

[7] S.M. Pingle, N.A. Fleck, V.S. Deshpande, et al., Collapse mechanism maps for a hollow pyramidal lattice, In: Proceedings of the Royal Society of London A: Mathematical, Physical and Engineering Sciences, p. rspa20100329.

[8] N. Wicks, J.W. Hutchinson, Optimal truss plates, Int. J. Solids Struct. 38 (2001) 5165–5183.

[9] W. Yuan, H.W. Song, C.G. Huang, Failure maps and optimal design of metallic sandwich panels with truss cores subjected to thermal loading, Int. J. Mech. Sci. 115 (2016) 56–67.

[10] W. Yuan, H.W. Song, C.G. Huang, Thermal post-buckling behavior of simply supported sandwich panels with truss cores, J. Therm. Stresses 39 (2016) 156–169.

[11] W. Yuan, H.W. Song, L.L. Lu, et al., Effect of local damages on the buckling behaviour of pyramidal truss core sandwich panels, Compos. Struct. 149 (2016) 271–278.

[12] W. Yuan, X. Wang, H.W. Song, et al., A theoretical analysis on the thermal buckling behavior of fully clamped sandwich panels with truss cores, J. Therm. Stresses 37 (2014) 1433–1448.

[13] M.J. Chen, Y.M. Pei, D.N. Fang, Multi-objective optimization design of radar absorbing sandwich structure, Appl. Math. Mech. 31 (2010) 339–348.

[14] T. Kim, H.P. Hodson, T.J. Lu, Fluid-flow and endwall heat-transfer characteristics of an ultralight lattice-frame material, Int. J. Heat Mass Trans. 47 (2004) 1129–1140.

[15] T. Kim, C.Y. Zhao, T.J. Lu, et al., Convective heat dissipation with lattice-frame materials, Mech. Mater. 36 (2004) 767–780.

[16] J. Singer, J. Arbocz, T. Weller, Buckling Experiments: Experimental Methods in Buckling of Thin-walled Structures, Shells, Built-up Structures, Composites and Additional Topics, John Wiley &Sons, 2002.

[17] R. Ansari, M.F. Shojaei, A.H. Shakouri, et al., Nonlinear bending analysis of first-order shear deformable microscale plates using a strain gradient quadrilateral element, Journal of Computational and Nonlinear Dynamics 11 (2016) 051014.

[18] T. Le-Manh, Q. Huynh-Van, T.D. Phan, et al., Isogeometric nonlinear bending and buckling analysis of variable-thickness composite plate structures, Compos. Struct. 159 (2017) 818–826.

[19] M. Rezaeifard, S.J. Salami, M.B. Dehkordi, et al., A new nonlinear model for studying a sandwich panel with thin composite faces and elastic-plastic core, Thin Wall Struct. 107 (2016) 119–137.

[20] S. Suresh, A. Mortensen, Functionally graded metals and metal-ceramic composites: Part 2, Thermomechanical behaviour, Int. Mater. Rev. 42 (1997) 85–116.

[21] H.S. Shen, Nonlinear bending response of functionally graded plates subjected to transverse loads and in thermal environments, Int. J. Mech. Sci. 44 (2002) 561–584.

[22] H.S. Shen, Nonlinear thermal bending response of FGM plates due to heat conduction, Compos. Part B: Eng. 38 (2007) 201–215.

[23] Y.H. Dong, Y.H. Li, A unified nonlinear analytical solution of bending, buckling and vibration for the temperature-dependent FG rectangular plates subjected to thermal load, Compos. Struct. 159 (2017) 689–701.

[24] H.Z. Zhong, Z.G. Yue, Analysis of thin plates by the weak form quadrature element method, Sci. China Phys. Mech. 55 (2012) 861–871.

[25] J. Singh, K.K. Shukla, Nonlinear flexural analysis of functionally graded plates under different loadings using RBF based meshless method, Eng. Anal. Bound Elem. 36 (2012) 1819–1827.

[26] G. Watts, S. Pradyumna, M.K. Singha, Nonlinear analysis of quadrilateral composite plates using moving kriging based element free Galerkin method, Compos. Struct. 159 (2017) 719–727.

[27] M. Cetkovic, Thermal buckling of laminated composite plates using layerwise displacement model, Compos. Struct. 142 (2016) 238–253.

[28] A. Mossavarali, M.R. Eslami, Thermoelastic buckling of plates

with imperfections based on a higher order displacement field, Journal of Thermal Stresses 25 (2002) 745–771.

[29] S.F. Nikrad, H. Asadi, Thermal postbuckling analysis of temperature dependent delaminated composite plates, Thin Wall Struct. 97 (2015) 296–307.

[30] H.S. Shen, Thermal postbuckling behavior of shear deformable FGM plates with temperature-dependent properties, Int. J. Mech. Sci. 49 (2007) 466–478.